On the inverse problem of blade design for centrifugal pumps and fans

2014 Inverse Problems 30 065003

(http://iopscience.iop.org/0266-5611/30/6/065003)

IOP Publishing Inverse Problems

Inverse Problems **30** (2014) 065003 (22pp) doi:10.1088/0266-5611/30/6/065003

On the inverse problem of blade design for centrifugal pumps and fans

N P Kruyt and R W Westra[1]

Department of Mechanical Engineering, University of Twente, PO Box 217, 7500 AE Enschede, The Netherlands

E-mail: n.p.kruyt@utwente.nl

Received 27 January 2014, revised 26 March 2014
Accepted for publication 9 April 2014
Published 19 May 2014

Abstract

The inverse problem of blade design for centrifugal pumps and fans has been studied. The solution to this problem provides the geometry of rotor blades that realize specified performance characteristics, together with the corresponding flow field. Here a three-dimensional solution method is described in which the so-called meridional geometry is fixed and the distribution of the azimuthal angle at the three-dimensional blade surface is determined for blades of infinitesimal thickness. The developed formulation is based on potential-flow theory. Besides the blade impermeability condition at the pressure and suction side of the blades, an additional boundary condition at the blade surface is required in order to fix the unknown blade geometry. For this purpose the mean-swirl distribution is employed. The iterative numerical method is based on a three-dimensional finite element method approach in which the flow equations are solved on the domain determined by the latest estimate of the blade geometry, with the mean-swirl distribution boundary condition at the blade surface being enforced. The blade impermeability boundary condition is then used to find an improved estimate of the blade geometry. The robustness of the method is increased by specific techniques, such as spanwise-coupled solution of the discretized impermeability condition and the use of under-relaxation in adjusting the estimates of the blade geometry. Various examples are shown that demonstrate the effectiveness and robustness of the method in finding a solution for the blade geometry of different types of centrifugal pumps and fans. The influence of the employed mean-swirl distribution on the performance characteristics is also investigated.

Keywords: turbomachines, centrifugal pumps and fans, blade design

(Some figures may appear in colour only in the online journal)

[1] Currently with FMC Separation Systems, Arnhem, The Netherlands.

1. Introduction

Turbomachines, and centrifugal pumps and fans in particular, are widely used in domestic and industrial situations to increase the pressure of fluids in order to facilitate fluid transport [9, 15]. Inside turbomachines, blades are present (see for example, figure 1 (left)) that direct the fluid flow and that give rise to energy transfer due to the pressure difference that exists between the two sides of rotating blades. Despite their long use, the design of the blades in these machines remains complex, due to the complex nonlinear governing equations, their complex three-dimensional shape and the contradictory design requirements.

When designing centrifugal pumps and fans, the main objective is to achieve efficient, lightweight and compact machines, while reducing the cost and duration of the design cycle. Advanced computer-aided design methods have been developed to support this design process. Current design methods employed in industry are classically based on empirical approaches, on simplified (one-dimensional or two-dimensional) flow analyses or on computational fluid dynamics computations that result in predictions of the hydraulic performance for a given blade geometry. This is the *direct approach* to the problem of blade design, in which the blade geometry is prescribed and the performance characteristics are computed. However, it is often difficult to determine which changes in geometry might lead to a desired, improved design, due to the complicated three-dimensional blade shapes and nonlinear effects.

Inverse-design methods are the counterpart of direct analysis methods. In inverse-design methods the hydraulic performance of a machine, for example in the form of a pressure distribution, is prescribed and the blade geometry is computed. The advantage of using such an inverse-design method is that a design of a turbomachine is obtained, which has the desired characteristics (performance, pressure distribution). The development of inverse-design methods for turbomachines employed knowledge developed for inverse-design of airfoils, as described in [16, 16].

In the past decades solution methods for the inverse problem of blade design have become increasingly popular in the field of turbomachinery. These methods can be classified by

- the dimensionality of the problem considered: two-dimensional [11, 13, 16, 18, 19, 21, 25, 30, 37, 40], quasi three-dimensional [26, 30] or three-dimensional [4, 5, 12, 13, 29, 37, 41, 43],
- whether the flow is considered to be: incompressible [4, 5, 19, 21, 26, 37] or compressible [10–13, 16, 18, 25, 30–30, 39–41, 43],
- the type of equations that are used to describe the flow: potential-flow equations [4, 5, 18, 19, 21, 26, 37, 43], Euler equations [12, 13, 25, 30, 39, 40], Euler equations with coupled boundary layer equations [16] or Reynolds-averaged Navier–Stokes equations (using simple turbulence models, such as algebraic mixing-length or Baldwin–Lomax model) [10, 11, 29, 30, 40, 41],
- the type of so-called loading that is employed: mean-swirl loading [4, 5, 19, 25, 26, 37, 43], pressure loading [10, 11, 13, 16, 21, 29, 30, 40, 41] or velocity loading [18],
- the type of turbomachines (see for example [15]) to which the method is applied: axial turbine [11–13, 18, 19, 21, 25, 26, 30, 30, 37, 40, 41], axial compressor (or pump or fan) [7, 10, 11, 13, 16, 19, 21, 29, 37], mixed-flow pump [3, 5, 45], radial turbine [4, 43], radial compressor [39, 44, 45].

The focus of the present study is on centrifugal pumps and fans, of different (sub)types, ranging from axial, to mixed-flow and radial rotors (these types are shown in more detail in section 6). For realistic applications, solution methods to inverse problems for these types of machines should be *three-dimensional*. The flow in centrifugal pumps and fans can generally

be considered as being *incompressible*, contrary to the flow in gas turbines and compressors. In these latter types of turbomachines the compressibility effects and the (potential) occurrence of shocks necessitates the use of flow models based on the Euler or (compressible) Reynolds-averaged Navier–Stokes equations. For centrifugal pumps and fans, the use of methods based on *potential-flow* equations is considered sufficient. These various flow considerations are discussed in more detail in section 3.

The objective of this study is to develop an inverse-design method that is suitable for the full range of subtypes, from axial, to mixed-flow and radial rotors, without modification. Contrary to compressors and turbines, centrifugal pumps generally have few blades (for pumps the number of blades is in the range 3–10, while for compressors the number of blades is up to 30). The method must provide for solutions, even in cases with few(er) blades where it is difficult to obtain solutions. In short, the method should be *robust*.

Existing methods for solving the three-dimensional inverse-design problem that are based on incompressible potential-flow theory are generally based on a Fourier expansion of the velocity potential in circumferential direction (for example [4, 5, 21, 26, 37]). Since vorticity is only present as vorticity bound to the blades, such Fourier series may suffer from Gibbs–Wilbraham phenomenon. For most applications reported in literature, the number of blades is rather high ($\geqslant$6). Some considerations on the Fourier-based methods are presented in appendix A.

In order to develop a robust method, an alternative approach is proposed here that is based on a careful selection of the boundary conditions that are applied in the iterative cycle. The discretization of the governing equations for potential flow is based on the three-dimensional finite element method.

The outline of this study is as follows. In section 2 the basics of centrifugal pumps and fans are summarized. Then the potential-flow model is discussed in section 3. In section 4 the inverse problem of blade design is formulated. The numerical approach is described in section 5. Examples of solutions to inverse-design problem are presented in section 6. Finally, findings from this study are discussed.

2. Basics of centrifugal pumps and fans

The coordinates of the camber surface of the blades can be expressed in Cartesian coordinates (x, y, z) or, more conveniently for centrifugal pumps and fans, in cylindrical coordinates (r, θ, z), where r is the radial distance (to the axis of rotation), θ is the azimuthal angle and z is the axial coordinate. The blade shape is generally determined in the following steps. Firstly, the so-called meridional shape, see also figure 1 (right), is determined that gives the basic shape of the flow channel. The meridional shape consists of the (r, z)-coordinates of the so-called hub and shroud surfaces of revolution (indicated in figure 1 (right)) and of the (r, z)-coordinates of the leading and the trailing edges (also indicated in figure 1 (right)). Secondly, to fully fix the geometry of the camber surface of the blades, the distribution of the azimuthal angle θ has to be determined on the blade surface. Thirdly, by incorporating a blade thickness distribution to the blade camber surface, a complete description of the geometry of the blades is obtained. The determination of the distribution of the azimuthal angle θ of the camber surface is the central problem in the inverse problem of blade design for centrifugal pumps and fans that is addressed here.

Hydraulic turbomachines, such as centrifugal pumps and fans where the flow can be considered as incompressible, are used to increase the total (or stagnation) pressure of the fluid. The total pressure p_0 consists of static pressure p and dynamic pressure $\frac{1}{2}\rho v^2$

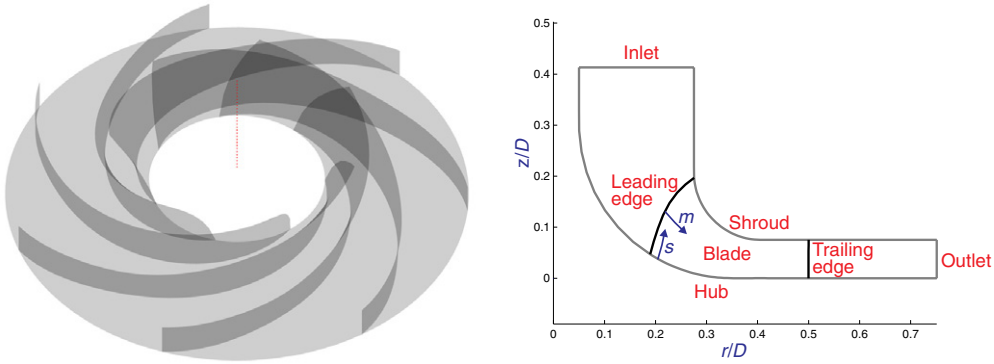

Figure 1. Left: example of a three-dimensional rotor with blades shown in dark grey; inlet, outlet and shroud surfaces are not shown for visual clarity. Right: meridional plane, giving (r, z)-coordinates; inlet, outlet, hub and shroud surfaces are indicated, as well as leading and trailing edges. Also indicated are the blade surface coordinates m in streamwise direction and s in spanwise direction. The diameter of the rotor is denoted by D.

$$p_0 = p + \tfrac{1}{2}\rho \mathbf{v}\cdot\mathbf{v}, \tag{1}$$

where ρ is the (constant) fluid density and $\mathbf{v}$ is the velocity vector. The total-pressure rise $\Delta p_0 = p_{0,\text{outlet}} - p_{0,\text{inlet}}$, from inlet to the machine to its outlet, is an important characteristic of hydraulic turbomachines. It is dependent on the operating conditions of the machine, i.e. the rotational (or angular) speed Ω and the volumetric flowrate Q through the machine. The size of the machine can be characterized by the diameter D of the rotor.

The performance, total-pressure rise Δp_0 as a function of rotational speed Ω and flowrate Q, can be expressed in terms of the non-dimensional flowrate φ , the non-dimensional pressure-rise ψ and the so-called specific speed N_s (see for example [15])

$$\varphi = \frac{Q}{\Omega D^3} \quad \psi = \frac{\Delta p_0}{\rho \Omega^2 D^2} \quad N_s = \frac{\Omega Q^{\frac{1}{2}}}{\left(\frac{\Delta p_0}{\rho}\right)^{\frac{3}{4}}}. \tag{2}$$

The specific speed N_s is a combination of the non-dimensional flowrate φ and the non-dimensional pressure-rise ψ such that it is independent of the diameter D of the machine.

Two frames of references may be convenient when considering the flow inside turbomachines, the stationary frame of reference and the frame of reference that rotates with the rotor at angular speed Ω. The velocity, i.e. the change in position of a fluid element, can be considered in the stationary frame of reference and in the rotating frame of reference. The corresponding velocities are the absolute velocity $\mathbf{v}$ and the relative velocity $\mathbf{w}$, respectively. These velocities are related by the so-called velocity triangle (see for example [15])

$$\mathbf{v} = \mathbf{w} + \mathbf{u} \quad \mathbf{u} = \boldsymbol{\Omega} \times \mathbf{r}, \tag{3}$$

where $\mathbf{u}$ is the local blade speed, $\boldsymbol{\Omega}$ is the angular speed vector and $\mathbf{r}$ is the position vector. In a cylindrical coordinate system the radial, circumferential and axial components of the absolute velocity $\mathbf{v}$ are denoted by v_r, v_θ, v_z, respectively. Similarly, the corresponding components of the relative velocity vector $\mathbf{w}$ are denoted by w_r, w_θ, w_z.

The basic equation that describes the energy transfer from (or to) the blades to (or from) the fluid is Euler's pump (or turbine) equation [15]

$$\frac{\Delta p_0}{\eta_h \rho} = \Omega(r_{\text{te}} v_{\theta,\text{te}} - r_{\text{le}} v_{\theta,\text{le}}), \tag{4}$$

where η_h is the hydraulic efficiency and subscripts le and te are used to denote quantities at the leading and trailing edges, respectively. Thus, the mean-swirl, rv_θ, at the leading and trailing edges is important for the total-pressure rise Δp_0.

3. Potential-flow model

The flow field, characterized by velocity field $\mathbf{v}$ and pressure field p, inside turbomachines can be described by the conservation laws of mass, momentum and energy, with appropriate boundary conditions. For the flow conditions mostly encountered in centrifugal pumps and fans, simplified flow equations can be formulated to capture the essential physics of the three-dimensional flow.

In the current study the incompressible potential-flow model is adopted, which is suitable for flows near the design point of the hydraulic machine [17, 22]. The potential-flow model is based on the assumptions of (i) inviscid flow, (ii) irrotational inflow and (iii) flow without boundary-layer separation. The assumption of inviscid flow is justified when the Reynolds number $Re = \frac{\Omega D^2}{\nu}$ (with ΩD as characteristic velocity, diameter D of the machine as characteristic length scale and ν the kinematic viscosity of the fluid) is large (typically $Re > 10^5$) and the turbulence intensity is small. The flow can be considered as incompressible when the Mach number $Ma = \frac{\Omega D}{a}$ (with a the speed of sound in the fluid) is small (typically $Ma < 0.2$) . With these assumptions the incoming irrotational flow remains irrotational, due to Kelvin's circulation theorem (see for example, [1]), i.e.

$$\nabla \times \mathbf{v} = 0. \tag{5}$$

Then the velocity vector $\mathbf{v}$ can be written as the gradient of a velocity potential ϕ

$$\mathbf{v} = \nabla \phi. \tag{6}$$

The incompressible mass conservation law, $\nabla \cdot \mathbf{v} = 0$, then becomes the Laplace equation for the velocity potential ϕ

$$\nabla^2 \phi = 0. \tag{7}$$

The conservation law of momentum can be simplified to the unsteady Bernoulli equation (see for example [1])

$$\frac{\partial \phi}{\partial t} + \frac{1}{2}\mathbf{v} \cdot \mathbf{v} + \frac{p}{\rho} = c(t). \tag{8}$$

The (generally time-independent) value of $c(t)$ is determined by the total pressure p_0 at inlet to the rotor.

Since the order of the governing equations is reduced by neglecting viscous terms, the no-slip condition at solid walls is not enforced. With the potential-flow model the flow *outside* of boundary layers can be described. These (thin) boundary layers will form at the rotor blades.

In the unsteady Bernoulli equation, equation (8), $\frac{\partial \phi}{\partial t}$ is the time derivative of the velocity potential in the stationary frame of reference. The time derivative of the velocity potential in the rotating frame of reference is denoted by $\frac{\partial \phi}{\partial t}_{|R}$. Since the material derivative $\frac{D\phi}{Dt}$ of a scalar quantity ϕ is objective (i.e. frame invariant), we have

$$\frac{\partial \phi}{\partial t} + \mathbf{v} \cdot \nabla \phi = \frac{D\phi}{Dt} = \frac{D\phi}{Dt}_{|R} = \frac{\partial \phi}{\partial t}_{|R} + \mathbf{w} \cdot \nabla \phi. \tag{9}$$

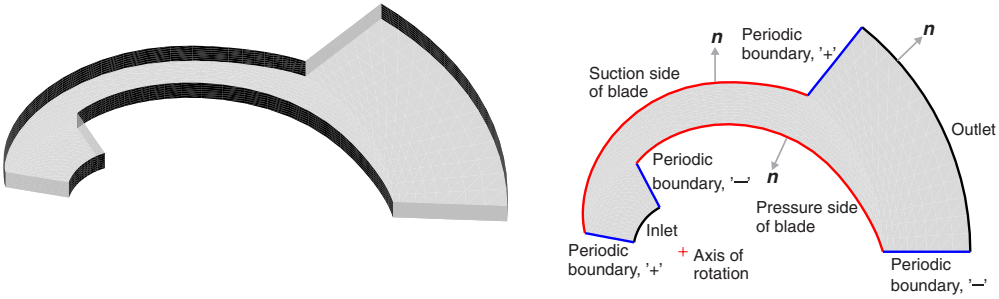

Figure 2. Left: single flow channel between two blades of a two-dimensional rotor; the shroud surface is not shown for visual clarity. Right: topology of flow channel; inlet and outlet surfaces, pressure and suction sides of the blades and periodic boundaries are shown. For realistic rotors, the inlet region is normal to the axis of rotation (as in figure 1). For visual clarity this is not the case in this schematic, quasi two-dimensional figure.

Hence, it follows that the time derivatives in the stationary and the rotating frame of reference are related by

$$\frac{\partial \phi}{\partial t}_{|R} = \frac{\partial \phi}{\partial t} + \mathbf{u} \cdot \nabla \phi, \tag{10}$$

where equation (3) has been used.

With a well designed diffuser, there will not be significant interaction between rotor and stationary parts of the machine at the design conditions. The flow field in the rotor is then *steady* in the rotating frame of reference, i.e. for an observer that rotates with the rotor

$$\frac{\partial \phi}{\partial t}_{|R} = 0. \tag{11}$$

Then the unsteady Bernoulli equation in the stationary frame of reference, equation (8), can be rewritten (after some algebra, using equations (3) and (10)) for the rotating frame of reference as

$$\frac{p}{\rho} + \frac{1}{2}\mathbf{w} \cdot \mathbf{w} - \frac{1}{2}\mathbf{u} \cdot \mathbf{u} = c(t). \tag{12}$$

This equation allows for the evaluation of the pressure p when the absolute velocity $\mathbf{v}$ (and hence the relative velocity $\mathbf{w}$) is known.

3.1. Domain of interest and boundary conditions

The blades are considered to be geometrically identical. When there is no interaction between rotor and stationary parts, the flow field in each of the channels between two consecutive blades is the same. Then it suffices to consider a single channel as the domain of interest where the flow solution is to be obtained, see for example figure 2 (left).

To solve the governing Laplace equation, equation (7), boundary conditions have to be formulated for the velocity potential ϕ at the boundary of the domain of interest. These boundary conditions will be given for the various surfaces that are indicated in figure 2 (right).

At the inlet surface, see figure 2 (right), it is assumed that the normal component of the velocity (given by $\frac{\partial \phi}{\partial n}$) is uniform. Its value is then determined from the specified flowrate Q

$$\frac{\partial \phi}{\partial n} = -\frac{Q}{A_{\text{inlet}}}, \tag{13}$$

where A_{inlet} is the area of the inlet surface to the turbomachine and the minus sign is present, since the inward velocity at the inlet is in the direction opposite to the outward unit normal vector $\mathbf{n}$.

Similarly, the boundary condition at the outlet surface is

$$\frac{\partial \phi}{\partial n} = +\frac{Q}{A_{\text{outlet}}}, \tag{14}$$

where A_{outlet} is the area of the outlet surface (see figure 2 (right)) to the turbomachine; here the outward velocity at the outlet is in the same direction as the outward unit normal vector $\mathbf{n}$.

At the impermeable hub and shroud surfaces (see figure 1 (right)) the normal component of the velocity is zero

$$\frac{\partial \phi}{\partial n} = 0. \tag{15}$$

At the pressure and suction sides of the blades, see figure 2 (right), the normal component of the relative velocity, $\mathbf{w}\cdot\mathbf{n}$, equals zero, since the blades are impermeable. Using equation (3), this blade impermeability condition can be expressed in terms of the velocity potential ϕ as

$$\frac{\partial \phi}{\partial n} = (\boldsymbol{\Omega} \times \mathbf{r}) \cdot \mathbf{n}. \tag{16}$$

Since the flow is considered to be identical in each of the flow channels between two blades, periodic boundary conditions can be formulated that relate the velocity vectors at corresponding surfaces. These corresponding surfaces are denoted as '+' and '−' surfaces in figure 2 (right). Periodic boundary conditions apply at the surfaces in front of the leading edges and behind the trailing edges. These conditions require that the velocity components normal and tangential to the surface at the corresponding surfaces are related. Hence

$$\frac{\partial \phi}{\partial n}_{|+} = -\frac{\partial \phi}{\partial n}_{|-} \qquad \phi_{|+} = \phi_{|-} + \gamma, \tag{17}$$

where γ is the distribution of the difference between the values of the potential at the '+' and '−' surfaces. The first relation states that the normal components of the velocity are equal; the minus sign is present, since the normal vectors at '+' and '−' surfaces are in opposite directions. The second relation states that the tangential components of velocity at the corresponding '+' and '−' surfaces are equal (refer to equation (6)). As the flow is assumed to enter the machine without pre-rotation, it follows that $\gamma = 0$ for the surfaces in front of the leading edge. To fix the values of γ for the surfaces behind the trailing edge, Kutta conditions are formulated [1, 8]. These conditions incorporate the essential effects of viscosity in an inviscid theory, as they enforce that the flow separates at the sharp trailing edge of the blades. Here the Kutta conditions are formulated as $\mathbf{w} \cdot \mathbf{n}_{|te} = 0$, or expressed in terms of the velocity potential ϕ as

$$\frac{\partial \phi}{\partial n}_{|\text{te}} = (\boldsymbol{\Omega} \times \mathbf{r}) \cdot \mathbf{n}_{|\text{te}}, \tag{18}$$

where the subscript te is used to indicate the value of a quantity at the trailing edge.

4. Formulation of inverse problem of blade design

For the complete formulation of the inverse problem of blade design, an additional condition at the blade surface is required, besides the Laplace equation equation (7) with boundary conditions as described in the previous section, in order to determine the distribution of the azimuthal angle $\theta(r, z)$ on the blade. This additional (so-called blade loading) condition should involve the desired performance characteristics of the centrifugal pump or fan, i.e. the increase Δp_0 of the total pressure as a function of angular speed Ω and the flowrate Q. The angular

speed Ω is present in the boundary condition equation (16) for the Laplace equation, while the flowrate Q is present in boundary conditions equations (13) and (14).

The Euler equation, equation (4), relates the increase of the total pressure Δp_0 to the values of the mean-swirl rv_θ at the leading and trailing edges. This suggests to use the *distribution* of the mean-swirl, from leading edge to trailing edge, as the additional condition required for the formulation of the inverse problem [4, 5, 19, 26, 37, 43]. This is described in more detail in the following subsection.

Alternative, more complex additional conditions can be formulated, such as a prescribed pressure difference between pressure and suction side of the blades or a prescribed, so-called velocity-loading distribution. These formulations have been investigated in [2, 10, 11, 13, 16, 18, 21, 29, 30, 40–42].

4.1. Mean-swirl distribution

The additional blade-loading condition employed here is that the mean-swirl distribution $r\overline{v}_\theta$ is prescribed

$$r\overline{v}_\theta = f(m, s), \tag{19}$$

where f is a function of the surface coordinates m and s in the streamwise and spanwise direction on the blade, respectively (as indicated in figure 1 (right)). The mean (or average) circumferential (absolute) velocity along a circular arc (with constant radius r) from blade to blade is defined by

$$\overline{v}_\theta = \frac{1}{\theta_{\mathrm{ss}} - \theta_{\mathrm{ps}}} \int_{\theta_{\mathrm{ps}}}^{\theta_{\mathrm{ss}}} v_\theta \, \mathrm{d}\theta \,, \tag{20}$$

where the subscripts ps and ss are used to indicate values at the pressure and suction side of the blades, respectively. For blades with infinitely small blade thickness as considered here, the difference in angle θ is determined by the number of blades Z: $\theta_{\mathrm{ss}} - \theta_{\mathrm{ps}} = \frac{2\pi}{Z}$. Hence it follows, using $v_\theta = \frac{1}{r}\frac{\partial \phi}{\partial \theta}$ (compare equation 6), that

$$\phi_{\mathrm{ss}} - \phi_{\mathrm{ps}} = \frac{2\pi}{Z} f \,. \tag{21}$$

Thus, a prescribed distribution of the mean-swirl $r\overline{v}_\theta$ is equivalent to the second relation for a periodic boundary condition (see equation (17)), where the '+' and '−' surfaces correspond to the suction and pressure side of the blade, respectively.

The incoming flow has no swirl, which means that $\gamma = 0$ in equation (17) at the periodic boundary in front of the leading edge. From the Euler relation, equation (4), it then follows that $\gamma = \frac{\Delta p_0}{\rho \Omega \eta_h}$ in equation (17) at the periodic boundary behind the trailing edge. Continuity of the difference in potential, $\phi_{|+} - \phi_{|-}$, is ensured when the mean-swirl distribution $f(m, s)$ satisfies the following constraints

$$f(m_{\mathrm{le}}, s) = 0 \quad f(m_{\mathrm{te}}, s) = \frac{\Delta p_0}{\rho \Omega \eta_h}. \tag{22}$$

Additional constraints for the mean-swirl distribution $f(m, s)$ follow from the condition that the flow angle (of the relative velocity) matches that of the blade, i.e. that the flow incidence is zero, and that the Kutta conditions, equation (18), are satisfied. These conditions are satisfied [4, 42] when

$$\frac{\partial f}{\partial m}(m_{\mathrm{le}}, s) = 0 \quad \frac{\partial f}{\partial m}(m_{\mathrm{te}}, s) = 0. \tag{23}$$

A simple, polynomial form for the mean-swirl distribution f that satisfies the constraints, equations (22) and (23), is

$$f(m,s) = \frac{\Delta p_0}{\rho\Omega\eta_h}[3\hat{m}^2 - 2\hat{m}^3] \quad \hat{m} = \frac{m - m_{\mathrm{le}}}{m_{\mathrm{te}} - m_{\mathrm{le}}}, \tag{24}$$

where $\hat{m}$ is the scaled (to the interval [0, 1]) streamwise coordinate m at the blade surface. A different choice for the mean-swirl distribution f will give a different solution to the inverse problem. Thus, the function $f(m, s)$ forms an important design parameter for the blades of centrifugal pumps and fans. This will be shown in detail in section 6.2.

4.2. Blade impermeability condition

The impermeability equation equation (16) involves the unit normal vector $\mathbf{n}$ at the blade surface, and hence the unknown distribution of the azimuthal angle θ at the blade surface. This normal vector is given by

$$\tilde{\mathbf{n}} = \frac{\partial \mathbf{x}}{\partial m} \times \frac{\partial \mathbf{x}}{\partial s} \tag{25}$$

where $\tilde{\mathbf{n}}$ is the unscaled normal vector (thus $\mathbf{n} = \tilde{\mathbf{n}}/\|\tilde{\mathbf{n}}\|$) and m and s are the surface parameters in the meridional plane (see also figure 1 (right)). After some algebra it follows that $\tilde{\mathbf{n}}$ can be expressed in cylindrical coordinates as

$$\tilde{\mathbf{n}} = r\left(\frac{\partial\theta}{\partial m}\frac{\partial z}{\partial s} - \frac{\partial\theta}{\partial s}\frac{\partial z}{\partial m}\right)\mathbf{e}_r + \left(\frac{\partial z}{\partial m}\frac{\partial r}{\partial s} - \frac{\partial z}{\partial s}\frac{\partial r}{\partial m}\right)\mathbf{e}_\theta + r\left(\frac{\partial r}{\partial m}\frac{\partial\theta}{\partial s} - \frac{\partial r}{\partial s}\frac{\partial\theta}{\partial m}\right)\mathbf{e}_z, \tag{26}$$

where $\mathbf{e}_r$, $\mathbf{e}_\theta$ and $\mathbf{e}_z$ are the unit vectors in radial, circumferential and axial directions, respectively.

The equation $\mathbf{w}\cdot\mathbf{n} = 0$ (or equivalently the equation $\mathbf{w}\cdot\tilde{\mathbf{n}} = 0$) can be rewritten, using the previous equation and the expression $\mathbf{w} = w_r\mathbf{e}_r + w_\theta\mathbf{e}_\theta + w_z\mathbf{e}_z$ for the relative velocity vector $\mathbf{w}$ in cylindrical coordinates, as the hyperbolic equation (when the relative velocity vector $\mathbf{w}$ is considered known) in the meridional plane

$$\frac{\partial\theta}{\partial m} = A(m,s)\frac{\partial\theta}{\partial s} + B(m,s) \tag{27}$$

with

$$A(m,s) = \frac{w_r\frac{\partial z}{\partial m} - w_z\frac{\partial r}{\partial m}}{w_r\frac{\partial z}{\partial s} - w_z\frac{\partial r}{\partial s}} \quad B(m,s) = \frac{w_\theta}{r}\left(\frac{\frac{\partial r}{\partial m}\frac{\partial z}{\partial s} - \frac{\partial z}{\partial m}\frac{\partial r}{\partial s}}{w_r\frac{\partial z}{\partial s} - w_z\frac{\partial r}{\partial s}}\right). \tag{28}$$

Since the meridional geometry, given by $r(m, s)$ and $z(m, s)$, is prescribed, the geometrical derivatives present in equation (28) are known.

As the hub and shroud surfaces are impermeable, the normal component of the velocity vector is zero there, as expressed by equation (15). The (non-scaled) normal vector to the hub and shroud surfaces of revolution is given by $\tilde{\mathbf{n}} = -\frac{\partial z}{\partial m}\mathbf{e}_r + \frac{\partial r}{\partial m}\mathbf{e}_z$. The condition $\mathbf{w}\cdot\tilde{\mathbf{n}} = 0$ then becomes $-w_r\frac{\partial z}{\partial m} + w_z\frac{\partial r}{\partial m} = 0$. Hence the function $A(m, s) = 0$ at the hub and shroud surfaces. Thus, the hub and shroud curves are characteristics of the partial differential equation (27) and it reduces to an ordinary differential equation here.

To solve equation (27), an 'initial' condition is required, for instance at the trailing edge in the form

$$\theta(m_{\mathrm{te}}, s) = \theta_{\mathrm{te}}(s). \tag{29}$$

This is the so-called stacking condition that determines the three-dimensional shape of the trailing edge.

In principle, the stacking condition can be prescribed at any curve in spanwise direction from hub to shroud. For turbines, the stacking condition is generally specified at the leading

edge of the blades. As the implementation of the inverse method is simpler when the stacking condition is applied at the trailing edge (or at the leading edge for turbines), such alternatives are not considered here.

4.3. Overview of inverse problem

Parameters that specify this inverse problem of blade design (for blades with infinitesimal blade thickness) consist of

- operating conditions for the design, i.e. angular speed Ω, flowrate Q and required total-pressure rise Δp_0, and (estimated) hydraulic efficiency η_h,
- meridional geometry, i.e. the hub and shroud contours and the position of leading and trailing edges of the blades,
- number of blades Z,
- mean-swirl distribution f,
- stacking condition θ_{te}.

Equations to be satisfied are

- governing Laplace equation, equation (7),
- boundary conditions equations (13)–(16) (or equivalently equations (27)) and (17),
- mean-swirl distribution, equation (19) (or equivalently equation (21)),
- stacking condition, equation (29).

Solution of the inverse problem consists of

- the distribution of the azimuthal angle θ at the blade surface, i.e. the missing geometrical quantity for the description of the camber surface of the blades
- the flow field, i.e. the velocity and pressure fields, $\mathbf{v}$ and p respectively, inside the rotor channel.

5. Numerical approach

As the blade geometry is not completely known, the domain of interest forms part of the solution to the inverse problem. Thus, the current problem is a free-boundary problem [23, 24, 31, 32, 34]. At the unknown boundary (i.e. the blade surface) the three boundary conditions are equation (19) (or equivalently equation (21)) and equation (16) at pressure and suction sides of the blades. Two classes of iterative numerical approaches can be distinguished for such free-boundary problems.

In the first, Picard-type class of methods [24, 34] the governing flow equations are solved on a fixed domain (which is based on the latest estimate of the blade geometry), where two of the three boundary conditions at the pressure and suction sides of the blades (i.e. at the free boundary) are enforced. The remaining boundary condition is then used to obtain a new estimate of the position of the free boundary, using (part of) the solution of the fixed-domain problem. This process is repeated, until convergence is obtained.

In the second, (quasi-)Newton-type class of methods [16, 23, 31, 32], the position of the free boundary is included in the linearized set of unknowns at each iteration step. Thus, the (linearized) influence of the geometrical unknowns on the governing flow equations has to be determined.

The advantage of the first class of methods is the (relative) simplicity of its implementation, while the advantage of the second class of methods is its higher rate of convergence in the iterative solution of the nonlinear equations.

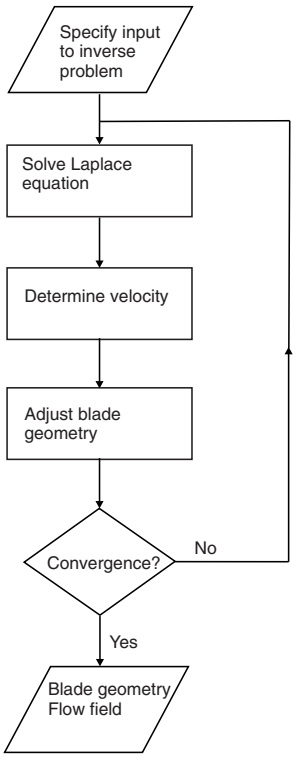

Figure 3. Flowchart of iterative scheme for solving the inverse problem.

Here the simpler, first approach is followed. The iterative approach consists of the solution of the Laplace equation equation (7), on a fixed domain with boundary conditions equations (13), (14), (15), (17) and (19).

Two boundary conditions are required at the pressure and suction sides of the blades for the flow solution on the fixed domain. The boundary conditions selected here are the prescribed mean-swirl distribution, equation (21), and the boundary condition $w_{n|+} = -w_{n|-}$, where the '+' and '−' surfaces correspond to the suction and pressure side of the blade, respectively. Since the corresponding points at the pressure and suction sides are located at the same radius r, it follows (using equation (3)) that this equation is equivalent to $v_{n|+} = -v_{n|-}$. Hence these boundary conditions at the blade surface are of the same type as the boundary conditions at the periodic boundaries in front and behind the blades, see equation (17).

Using the solution obtained for the relative velocity vector $\mathbf{w}$ at the blade surface (either at the pressure side or at the suction side), the blade geometry is adjusted, based on the solution of equation (27) with the stacking condition equation (29). This process is repeated until convergence is obtained. The flowchart for this iterative scheme is illustrated in figure 3.

The boundary conditions described above for the intermediary solutions (on the fixed domain) in the iterative process are always consistent with overall mass conservation requirement, $\int_S v_n \, \mathrm{d}S = 0$, where S is the boundary of the domain of interest.

When the solution satisfies the impermeability condition $\mathbf{w} \cdot \mathbf{n} = 0$, at either the pressure side or at the suction side, then the imposed boundary condition $w_{n|+} = -w_{n|-}$ ensures that the solution satisfies the impermeability condition at pressure *and* suction sides of the blades.

5.1. Implementation and additional numerical techniques

Here a finite element method approach is adopted to solve the Laplace equation, equation (7), for the velocity potential ϕ with linear tetrahedral elements. This gives second-order accuracy for the velocity potential ϕ. Some details on the weak form of the Laplace equation in the presence of periodic boundary conditions and their handling in the discretization are described in appendix B.

Although here a finite element method is employed (based on the authors' experience), finite volume, finite difference or boundary integral methods could also be used to solve the governing Laplace equation. A critical factor for the method to be robust is the suitable formulation of the boundary conditions for the intermediate flow solutions in the iterative process, as described before.

In each iteration a structured finite element mesh is generated automatically, where each elementary cube is subdivided into six tetrahedra. This structured-mesh approach is employed, as the mesh generation process is easily automated. The structured mesh is refined in circumferential direction near the blades and in streamwise direction near the leading and trailing edge locations.

The absolute velocity vector $\mathbf{v}$, i.e. the gradient of the potential ϕ, in the nodal points is determined from the nodal point values of the potential using the SPR-method [47], as it gives better accuracy for the velocity vector in comparison with other post-processing methods. The accuracy is second-order (for the linear elements employed) for internal nodes, while for boundary nodes the order of accuracy is lower. The relative velocity vector $\mathbf{w}$ in the nodal points is determined from the absolute velocity vector $\mathbf{v}$, using the velocity triangle equation (3).

The equation employed for the adjustment of the blade geometry, the impermeability condition equation (27), is discretized using the implicit second-order (in space) Crank–Nicholson scheme

$$\frac{\theta_{i+1,j}-\theta_{i,j}}{\Delta m}=\frac{A_{i+1,j}(\theta_{i+1,j+1}-\theta_{i+1,j-1})+A_{i,j}(\theta_{i,j+1}-\theta_{i,j-1})}{4\Delta s}+\frac{B_{i+1,j}+B_{i,j}}{2}, \tag{30}$$

where i is the index in the streamwise m-direction and j is the index in the spanwise s-direction. These equations are solved from the trailing edge, where the stacking condition equation (29) provides the starting values, towards the leading edge. Note that these discrete equations are *coupled* in the spanwise s-direction. This coupling of the equations for the adjustment of the blade geometry, as determined by the distribution of the angle θ, is very important for the increased robustness of the proposed method, in comparison with line-based methods, as employed in [26].

In principle, the velocities at pressure side or at the suction side could be employed in equation (4). Since the relative velocity at the pressure side is lower than at the suction side (due to the existence of the so-called counter-vortex), backflow is more likely to occur at the suction side than at the pressure side (especially in the intermediate flow solution encountered in the iterative process). Backflow is associated with a divergence of the quantity $A(m, s)$ in equation (16). Therefore the velocities at the suction side are always used for the adjustment of the blade geometry.

Using this approach, an adjusted blade geometry, as characterized by the solution $\theta_{i,j}^{\mathrm{adj}}$ of equation (30), is obtained. However, in order to achieve convergence of the iterative process, it is often beneficial to limit the maximum change $\theta_{i,j}^{\mathrm{adj}}-\theta_{i,j}^{n}$ in the blade angles to a maximum (absolute) value, $\Delta\theta_{\max}$. Here $\theta_{i,j}^{n}$ denotes the previous estimate of the azimuthal angles of the blade surface. This change-in-angle limitation is especially beneficial in the initial stage of the iterative process and when the initial estimate deviates strongly from the solution to the inverse problem.

An additional technique for increasing the robustness of the method is to employ under-relaxation. The new estimate of the azimuthal angles, $\theta_{i,j}^{n+1}$ is obtained from the previous estimate $\theta_{i,j}^{n}$ and the adjusted solution $\theta_{i,j}^{\mathrm{adj}}$ by

$$\theta_{i,j}^{n+1} = \theta_{i,j}^{n} + \omega\left(\theta_{i,j}^{\mathrm{adj}} - \theta_{i,j}^{n}\right), \tag{31}$$

where $\omega < 1$ is the under-relaxation coefficient.

The convergence criterion employed for the iterative process is that the magnitude of the flowrate through the blades (which should be equal to zero, see equation (16)) is smaller than a specified fraction (typically 0.1%) of the flowrate Q through the machine. Typical convergence histories are given in [42].

The complete method has been tested and verified for a simple two-dimensional case of a source and free vortex flow. For this case an analytical solution is available (see [42]). The computational cost of the current method and of the Fourier-based method [4] is comparable when efficient iterative methods (such as multigrid methods) are employed to solve the discretized equations.

In consideration of the order of accuracy of the complete method, solutions to the inverse problem have been computed using three different meshes with increasing number of nodes. The position of the leading edge from these solutions has been compared. Using Richardson extrapolation, the order of accuracy of the complete method is found to equal 1.1, see [42] for more details. This relatively low order of accuracy of the complete method is attributed to the lower order of accuracy of the SPR-method for the velocities at the blade surfaces. The velocities obtained through the use of the SPR-method at the blades are required in the solution of the equation for the adjustment of the blade geometry, equation (27).

5.2. Initial estimate of geometry, existence and uniqueness of solutions

An initial estimate of the blade geometry is required for the iterative solution method. This initial estimate can be determined in a number of ways. Firstly, by estimating the blade geometry at the leading and trailing edges, assuming that the flow field is uniform from blade to blade (see for example [15]). In between leading and trailing edges, the initial blade geometry is then interpolated. Secondly, the meridional velocities can be computed by analysing the flow field in the absence of rotor blades. This gives estimates of the radial and axial velocity components w_r and w_z. The circumferential velocity component w_θ is estimated from the mean-swirl distribution equation (19) (which gives the average circumferential component of the absolute velocity v_θ) and from the velocity triangle equation (27). Using this approximate relative velocity field, the blade adjustment equation (30) can be solved to give the initial estimate for the blade geometry. The developed method is not very sensitive to the quality of the initial estimate: even when the difference between the initial and the final blade shape is large, a solution is generally found. The number of iterations that is required is, of course, smaller when a good initial estimate is employed.

For airfoils it is known that constraints need to be satisfied by the prescribed pressure distribution for solutions to inverse problems to exist, see for example [24]. The issue of existence and uniqueness of solutions to inverse problems for turbomachines is also discussed (for the two-dimensional case) in [25].

From experience in the design of centrifugal pumps and fans it is known (see for example [15]) that there is a correlation between the meridional shape and the specified performance characteristics, i.e. angular speed Ω, flowrate Q and total-pressure rise Δp_0. For a high value of the so-called specific speed N_s (see equation (2)), efficient designs are possible when the meridional shape is axial, while a radial meridional shape is best for low values of

the specific speed (see also section 6 for a description of these meridional shapes). This also suggests that solutions to the inverse problem of blade design do not always exist, although no proof is available.

From experience with the developed method when using different initial estimates, it appears that the same solution (when found) is obtained, irrespective of the initial estimate. This suggests that the solution is unique (when it exists), although no proof is available.

6. Examples

To demonstrate the capabilities of the developed method, firstly some examples are shown in section 6.1 of solutions to the inverse-problem that correspond to different values of the specific speed N_s, see equation (2). Secondly, the influence of the mean-swirl distribution $f(m, s)$, which constitutes an input parameter for the designer, on various performance characteristics is investigated in section 6.2.

6.1. Different types of rotor

The developed solution method for the inverse problem has been applied to three different cases. These cases correspond to three different types of rotor: (i) a radial type, (ii) a mixed-flow type and (iii) an axial type. These cases correspond to different meridional geometries, as shown in the left column of figure 4. The specified operation conditions (expressed in terms of the dimensionless flow coefficient φ, dimensionless total-pressure rise coefficient ψ and dimensionless specific speed N_s, see equation (2)), meridional geometries and number of blades Z were based on existing designs.

In all three cases the mean-swirl distribution according to equation (24) has been used, without a stacking distribution (i.e. the blade is straight in spanwise direction at the trailing edge). For the radial rotor $\phi = 0.014$, $\psi = 0.141$, $N_s = 0.51$ and $Z = 7$. For the mixed-flow rotor $\phi = 0.039$, $\psi = 0.087$, $N_s = 1.24$ and $Z = 5$. For the axial rotor $\phi = 0.106$, $\psi = 0.017$, $N_s = 6.96$ and $Z = 6$.

For the structured computational grids the number of nodes employed are 78, 35 and 15 in streamwise direction, from blade to blade and in spanwise direction, respectively. Values for parameters in the robustness-enhancing techniques are the under-relaxation coefficient $\omega = 0.3$ and the maximum change-in-angle $\Delta\theta_{\max} = 25^\circ$. The required number of iterations ranged from 17–26 (higher for the radial case than for the axial case).

The method yields a solution to these different inverse problems, without modifications. This shows the robustness of the developed method.

For these three meridional geometries, the number of blades Z was varied to determine the lowest number of blades, $Z_{\min}$, for which a solution to the inverse problem could still be obtained (through reduction of the under-relaxation coefficient ω and the maximum change-in-angle $\Delta\theta_{\max}$). The minimum number of blades were: $Z_{\min} = 4$ for the radial rotor, $Z_{\min} = 3$ for the mixed-flow rotor and $Z_{\min} = 3$ for the axial rotor. Note that these solutions do not necessarily correspond to good designs from the hydrodynamical viewpoint, as they show small or negative (i.e. backflow) velocities at the pressure side of the blades. However, the fact that solutions with few blades could be obtained further emphasizes the robustness of the developed method. In the literature examples are presented with many blades (generally $Z \geqslant 6$).

6.2. Influence of mean-swirl distribution

The influence of the mean-swirl distribution $f(m, s)$ on various performance characteristics is investigated here. These performance characteristics are: (i) power losses, (ii) cavitation

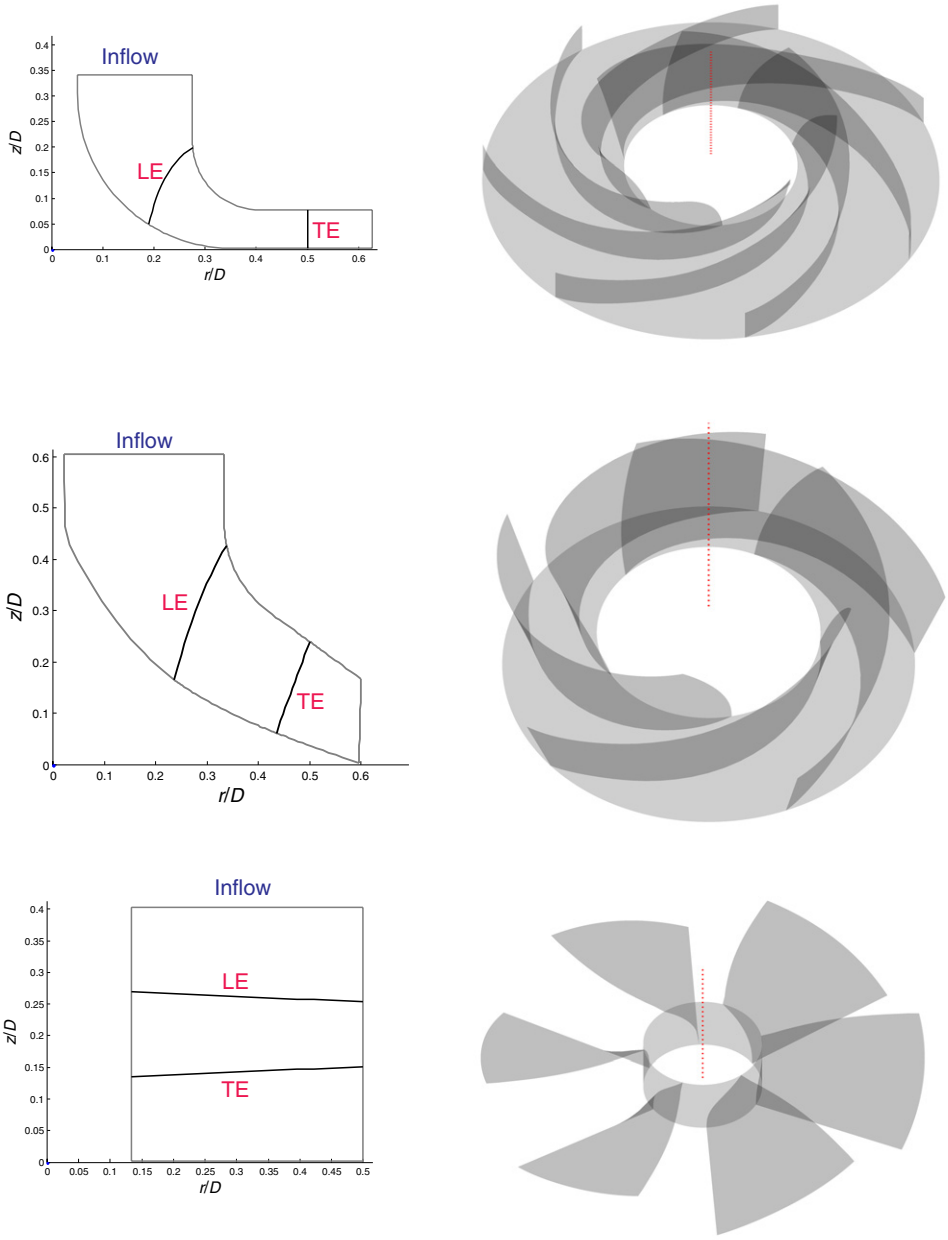

Figure 4. Left column: meridional plane used as input; indicated are inflow regions, leading edges (LE) and trailing edges (TE). Right column: resulting rotor geometries. Top row: radial rotor ($N_s = 0.51$). Middle row: mixed-flow rotor ($N_s = 1.24$). Bottom row: axial rotor ($N_s = 6.96$).

inception coefficient and (iii) velocity loading. These performance characteristics will now be described.

The power losses ΔP are estimated, based on the inviscid velocity field. This velocity field at solid surfaces, such as blades, hub and shroud surfaces, represents the velocity at the

edge of the boundary layers that form at these surfaces. Using this velocity field, the power loss inside boundary layers can be estimated by [14, 33]

$$\Delta P = \frac{1}{2}\rho c_D \int_S w^3 \mathrm{d}S\,, \tag{32}$$

where c_D is a dissipation coefficient (in the range 0.003–0.005; its value is fairly insensitive to the state of the boundary layer), S is the solid area where the boundary layer forms (i.e. at pressure and suction sides of the blades and at the hub and shroud surfaces) and w is the magnitude of the (potential-flow) relative velocity vector $\mathbf{w}$. The fraction of power loss ΔP over the power input P_{input} is the loss coefficient ζ

$$\zeta = \frac{\Delta P}{P_{\text{input}}}\,. \tag{33}$$

The power input P_{input} is easily determined from the inviscid potential-flow computation by $P_{\text{input}} = P_{\text{output}} = Q\Delta p_0$.

Cavitation (see for example [6]) is the phase transition from liquid to *vapour* phase due to acceleration of the flow, which may occur in centrifugal pumps (not in fans where the medium is a gas). In general, the occurrence of cavitation is undesirable. Close to the leading edge of the blades the flow (locally) accelerates, resulting in a drop in pressure p. When the local pressure drops below the vapour pressure p_{vapour}, vapour bubbles will form. This will be the case when the inlet pressure is low and/or the local acceleration is large. Further downstream in the machine, where the pressure is higher, these vapour bubbles will collapse violently, resulting in damage to the blades. Additionally, cavitation can lead to a decrease in total-pressure rise and/or efficiency. The dimensionless cavitation coefficient κ describes the margin between the total pressure at the inlet that is required in order to prevent cavitation bubbles from forming, $p_{0,\text{inlet, no bubble}}$, and the vapour pressure p_{vapour}. This is a cavitation inception criterion. The dimensionless cavitation inception coefficient κ is defined by

$$\kappa = \frac{p_{0,\text{inlet, no bubble}} - p_{\text{vapour}}}{\frac{1}{2}\rho u_{te}^2}\,, \tag{34}$$

where u_{te} is the (maximum) blade speed at the trailing edge. A low cavitation coefficient κ is desirable, as it allows for operation of the centrifugal pump without cavitation at low inlet pressures (i.e. without strong requirements for the total pressure at the inlet).

The dimensionless velocity loading coefficient χ is frequently used to describe the performance of centrifugal pumps and fans [35, 36, 38]. This coefficient describes the tendency for boundary layers to separate when the flow deceleration along the blades is large: a low value for the velocity loading coefficient χ is favourable. The velocity loading coefficient χ is defined by

$$\chi = \frac{w_{\text{ss}} - w_{\text{ps}}}{\frac{1}{2}(w_{\text{ss}} + w_{\text{ps}})}\,, \tag{35}$$

where w_{ss} and w_{ps} are the magnitudes of the relative velocities at the suction and pressure sides of the blades, respectively. The velocity loading coefficient χ is the ratio between the difference between these relative velocities over their mean. At the suction side the relative velocity will be high, compared to that at the pressure side, see also equation (12). When the relative velocity at the pressure side becomes almost zero (corresponding to the initiation of backflow), the velocity loading coefficient equals 2. A guideline is that the velocity loading coefficient χ should be smaller than 0.7–1.5, depending on the specific speed N_s [35, 36].

The mean-swirl distribution is described here in a simple, *single-parameter* form to demonstrate that different mean-swirl distributions result in solutions (i.e. geometries of rotor

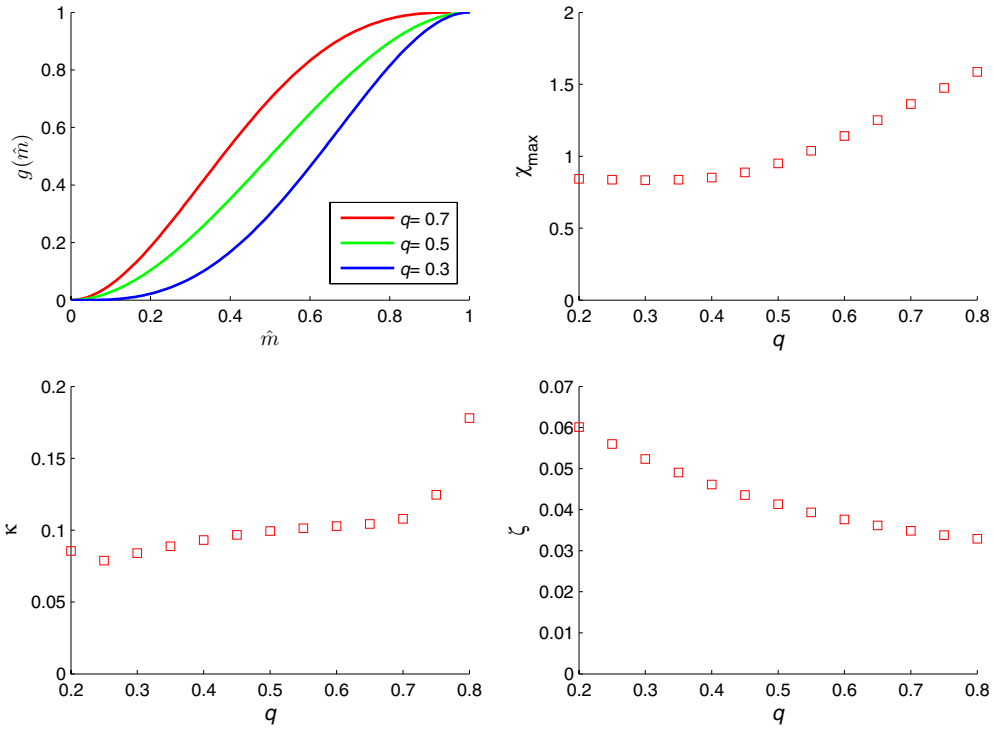

Figure 5. Influence of mean-swirl distribution $f(m, s)$ on performance characteristics. Top left: scaled mean-swirl distribution $g(\hat{m}) \equiv f(\hat{m})\,[\rho\Omega\eta_h/\Delta p_0]$ $(0 \leqslant g(\hat{m}) \leqslant 1)$ as a function of the scaled meridional coordinate $\hat{m}$ according to equation (36), for various values of the single parameter q. Top right: maximum (over the blades) velocity loading coefficient $\zeta_{\max}$ as a function of the parameter q. Bottom left: cavitation inception coefficient κ as a function of the parameter q. Bottom right: loss coefficient ζ as a function of the parameter q.

blades) with different performance characteristics. This mean-swirl distribution function is given by a quartic polynomial (also employed in [7])

$$f(m, s) = \frac{\Delta p_0}{\rho\Omega\eta_h}[(16q - 5)\hat{m}^2 + (14 - 32q)\hat{m}^3 + (16q - 8)\hat{m}^4]\,, \tag{36}$$

where the scaled streamwise coordinate in the meridional plane $\hat{m}$ is given in equation (24). Note that this distribution satisfies the constraints on the mean-swirl distribution given in equations (22) and (23) for all values of q and that for $q = 1/2$ the mean-swirl distribution given in equation (24) is retrieved.

The single parameter q has been varied for the mixed-flow meridional geometry (i.e. the second case in section 6.1). Some corresponding mean-swirl distributions are shown in figure 5 (top left). For each case, i.e. each value for q, the inverse problem was solved, using the numerical method described in section 5, and the performance characteristics given in this subsection were determined from the solution to the inverse problem. The results are shown in figure 5, which illustrates the influence of the mean-swirl distribution on the performance characteristics. The maximum (over the blade) velocity loading $\chi_{\max}$ is shown at the top right, the cavitation inception coefficient κ at the bottom left and the loss coefficient ζ at the bottom right (for $c_D = 0.004$). Note that the total-pressure rise Δp_0 is the same for all these cases.

For comparison, the values of the hydraulic characteristics of the original rotor design have also been computed (using a direct solver for the potential-flow problem). These values are: $\chi_{\max} = 1.46, \kappa = 0.22$ and $\zeta = 0.038$. In comparison to the original design the inverse designs have much better cavitation behaviour (low cavitation coefficient κ) and lower (maximum) velocity loading coefficient $\chi_{\max}$. The losses, characterized by ζ, are generally somewhat higher. To obtain inverse designs with low(er) losses while retaining the other, favourable performance characteristics, more complicated (described by more than a single parameter) mean-swirl distributions have to be considered (see [42]). More detailed descriptions of the original and the resulting geometries are reported in [42] where the so-called blade-angle distributions are shown that describe the blade geometry.

For an acceptable value of the (maximum) velocity loading coefficient, $\chi_{\max} < 1$ for mixed-flow machines, the value of q should be smaller than 0.5. With an increase in q, the loading changes from front-loading to aft-loading of the blades. Front-loaded blades are shorter, but give a more pronounced pressure drop near the leading edge than aft-loaded blades. Hence, front-loaded blades have lower losses (due to the smaller surface areas, compare equation (32)), but worsened cavitation properties in comparison to aft-loaded blades. The results shown in figure 5 demonstrate that the desirable performance characteristics of low loss coefficient ζ, low cavitation coefficient κ and low (maximum) velocity loading coefficient $\chi_{\max}$ are contradictory. Similar trends for the dependence of losses and cavitation characteristics on variations in the blade loading were observed in [3].

The presented variation of the parameter q represents a limited sensitivity analysis, where the hydraulic parameters are used to characterize the solution. The results shown in figure 5 indicate that the solution (i.e. the hydraulic characteristics) generally depends continuously on parameter q. Thus, in this sense this inverse problem seems to be generally well-posed. However, the cavitation inception coefficient κ rapidly increases for q in the range 0.75–0.80. This gives an indication of loss of well-posedness. The geometry of the rotors, that forms part of the solution to the inverse problem, is sensitive to the prescribed mean-swirl distribution (see [42]).

7. Discussion

The inverse problem of blade design for centrifugal pumps and fans has been studied. Based on potential-flow theory, the inverse problem has been formulated, in which the meridional coordinates (r, z) are specified and the distribution of the azimuthal angle $\theta(r, z)$ constitutes an additional unknown, next to the flow field. Besides the governing Laplace equation with appropriate boundary conditions, an additional boundary condition has been employed, the mean-swirl distribution, in order to fix the unknown blade geometry.

An iterative numerical method has been developed to solve the inverse problem. This is based on a Picard-type of approach, in which the Laplace equation is solved on an estimated domain, with some of the boundary conditions at the blade surface being enforced. The remaining boundary condition at the blade surface is used to find an improved estimate of the blade shape. This process is repeated until convergence is obtained.

The robustness of the method is increased significantly by employing a number of techniques: (i) the suitable formulation of boundary conditions for the intermediate flow solutions (which are obtained through a finite element method for the discretization of the Laplace equation) in the iterative process, (ii) the coupled discretization of the impermeability condition, equation (30), (iii) the use of under-relaxation in the adjustment of the blade geometry and (iv) the use of a maximum change-in-angle between successive estimates of

the blade angle θ. These extra techniques have proven to be essential in obtaining converged solutions for a wide variety (expressed through the specific speed, N_s) of rotors (as shown in section 6.1) and for a range of prescribed mean-swirl distributions (as shown in section 6.2). Specifically, solutions can (also) be found for low numbers of blades, Z.

The developed method gives the azimuthal angle θ at the blade surface (as part of the solution), where the meridional geometry forms input to the method. This input of the meridional geometry remains largely due to experience (and is related to the specific speed N_s).

The method gives a blade geometry, based on considerations at a *single* operation point. A consequence is that the obtained design may perform well at this design point, but the performance may degrade (rapidly) when the centrifugal pump or fan is operated at conditions (flowrate Q or angular speed Ω) that deviate from the design conditions. To alleviate this situation, the method for solving the inverse problem could be employed as part of an optimization method, in which blade geometries under consideration are solutions of the inverse problem (see for example [27, 42]). In this hybrid manner (combining solutions of inverse problems with results of optimization methods) the performance at off-design conditions may be taken into account in the design process.

The present method has been developed for blades of infinitesimal thickness. Some work on extending the method to the case with finite blade thickness, while maintaining a true representation of the geometry during the flow solution, is reported in [2] for the two-dimensional case. The extension towards the three-dimensional case is presently under investigation. With infinitesimal blade thickness a non-zero angle of incidence gives rise to a weak singularity near the leading edge (see for example [1]). In design practice, some flow incidence is sometimes aimed for, even at the design point. By considering the case with finite blade thickness, an inverse problem can be formulated that allows for flow incidence at the leading edge, but that does not involve a weak singularity.

The current method is based on a Picard-type method, in which the solutions for the flow field and for the geometry are decoupled at the stage of a single iteration. To increase the convergence rate of the method, it may be beneficial to develop the more complex (quasi-) Newton methods, as have been reported for viscous free-boundary problems [23, 31, 32] and used in [16] for two-dimensional inverse-design problems for turbomachines.

Acknowledgments

The authors acknowledge financial support from the Dutch Technology Foundation (STW) for the project *Inverse-design and optimization methods for centrifugal pump impellers and fans*(TSF.6157). The authors thank the companies involved, i.e. Flowserve, IHC, Johnson Pump (currently SPX), Marin, NLR and Urenco Aerospace (currently Aeronamics), for valuable discussions.

Appendix A. Considerations on Fourier-based methods for inverse problem of blade design

The methods for the inverse problem by [4, 5, 21, 26, 37] are based on a Fourier expansion for the potential ϕ in circumferential direction θ. This leads to (indefinite) two-dimensional inhomogeneous Helmholtz equations for the Fourier amplitudes of the potential in the meridional plane (see [4]). It is well-known that such solutions of Helmholtz equations are strongly oscillatory for high 'wave numbers' (see for example [20]). Furthermore, the right-hand side in the inhomogeneous Helmholtz equations is strongly oscillatory for higher Fourier

modes. These factors may contribute to the convergence problems in the overall iterative Fourier-based methods.

In the method proposed here the boundary conditions for the intermediate flow solutions in the iterative cycle are selected such that the normal component of the velocity at the pressure side and the suction side of the blades satisfy the condition $\frac{\partial\phi}{\partial n}_{|+} = -\frac{\partial\phi}{\partial n}_{|-}$. Hence, the intermediate flow solutions satisfy the overall (integral) form of the mass conservation equation, equation (7). Such consistency is not generally ensured for the methods based on Fourier expansions. This means that those intermediate solutions generated during the iterative process may violate the overall (integral) form of the mass conservation equation, equation (7). This may be a source of convergence problems.

The Fourier-based methods were developed for blades with infinitesimal thickness. The generalization of such methods to blades with finite blade thickness is not possible when an accurate representation of the blade geometry and of the flow field is required. Such an accurate representation is required for proper evaluation of cavitation characteristics, which are determined by the flow near the leading edge of the blades. For the FEM-based methods an accurate representation of the blade geometry and an accurate flow solution is possible for blades with finite thickness (see [2] for the two-dimensional case).

Appendix B. Weak form of Laplace equation and handling of periodic boundary conditions

The weak form of the Laplace equation, equation (7), forms the basis of discretization by the finite element method. Here this weak form is shortly described, with emphasis on the treatment of the periodic boundary conditions, equation (17).

The weak form of the Laplace equation (7) is obtained by multiplication by an arbitrary test function ψ that satisfies the periodicity constraints $\psi_{|S_+} = \psi_{|S_-}$ and by integration over the domain of interest V. Using Gauss theorem, it follows that

$$\int_V \nabla\phi \cdot \nabla\psi \, \mathrm{d}V = \int_{S_N} \frac{\partial\phi}{\partial n}\psi \, \mathrm{d}S + \int_{S_+} \frac{\partial\phi}{\partial n}\psi \, \mathrm{d}S + \int_{S_-} \frac{\partial\phi}{\partial n}\psi \, \mathrm{d}S \,, \tag{B.1}$$

where S_N is the part of the boundary where Neumann boundary conditions ($\frac{\partial\phi}{\partial n} = v_n$) apply and S_+ and S_- are corresponding surfaces in the periodic boundary conditions. Since the test function ψ is required to be periodic, $\psi_{|S_+} = \psi_{|S_-}$, and the normal components of the velocity satisfy the first relation in equation (17), the terms corresponding to the periodic boundaries cancel out. The final expression for the weak form of the Laplace equation becomes

$$\int_V \nabla\phi \cdot \nabla\psi \, \mathrm{d}V = \int_{S_N} v_n\psi \, \mathrm{d}S \,. \tag{B.2}$$

The degrees of freedom, represented as a vector, can be divided into those for periodic surfaces at S_+ and S_-, with vectors $\{\boldsymbol{\phi}^+\}$, $\{\boldsymbol{\phi}^-\}$ respectively, and remaining degrees of freedom $\{\boldsymbol{\phi}^i\}$. The discretization by the finite element method gives a system of equations of the following structure, where the various submatrices $\mathbf{L}$ describe the coupling between the various sets of degrees of freedom. The right-hand side vector can be grouped in a similar manner. The discretized linear system of equations can then be written as

$$\begin{bmatrix} [\mathbf{L}^{ii}] & [\mathbf{L}^{i-}] & [\mathbf{L}^{i+}] \\ [\mathbf{L}^{-i}] & [\mathbf{L}^{--}] & [\mathbf{L}^{-+}] \\ [\mathbf{L}^{+i}] & [\mathbf{L}^{+-}] & [\mathbf{L}^{++}] \end{bmatrix} \begin{Bmatrix} \{\boldsymbol{\phi}^i\} \\ \{\boldsymbol{\phi}^-\} \\ \{\boldsymbol{\phi}^+\} \end{Bmatrix} = \begin{Bmatrix} \{\boldsymbol{R}^i\} \\ \{\boldsymbol{R}^-\} \\ \{\boldsymbol{R}^+\} \end{Bmatrix} . \tag{B.3}$$

The degrees of freedom vectors at the periodic surfaces S_+ and S_- are related by $\{\boldsymbol{\phi}^+\} = \{\boldsymbol{\phi}^-\} + \{\gamma\}$, see the second relation in equation (17). Hence, the degrees of freedom

$\{\boldsymbol{\phi}^+\}$ can be eliminated from the system of equations. This can be done, while preserving the symmetry properties of the original discretization in equation (B.3), by adding the third block of equations to the second block of equations. The final result for the discretized system of linear equations is

$$\begin{bmatrix} [\mathbf{L}^{ii}] & [\mathbf{L}^{i-}] + [\mathbf{L}^{i+}] \\ [\mathbf{L}^{-i}] + [\mathbf{L}^{+i}] & [\mathbf{L}^{--}] + [\mathbf{L}^{++}] + [\mathbf{L}^{-+}] + [\mathbf{L}^{+-}] \end{bmatrix} \begin{Bmatrix} \{\boldsymbol{\phi}^i\} \\ \{\boldsymbol{\phi}^-\} \end{Bmatrix} = \begin{Bmatrix} \{\boldsymbol{R}^i\} - [\mathbf{L}^{i+}]\{\gamma\} \\ \{\boldsymbol{R}^+\} + \{\boldsymbol{R}^-\} - ([\mathbf{L}^{-+}] + [\mathbf{L}^{++}])\{\gamma\} \end{Bmatrix}. \tag{B.4}$$

References

[1] Batchelor G K 1967 *An Introduction to Fluid Dynamics* (Cambridge: Cambridge University Press)
[2] Bijleveld H A 2007 Inverse design method for centrifugal pump impellers: new blade loadings and incorporation of blade thickness *MSc Thesis* Department of Mechanical Engineering, University of Twente, Enschede, The Netherlands
[3] Bonaiuti D, Zangeneh M, Aartojarvi R and Eriksson J 2010 Parametric design of a waterjet pump by means of inverse design, CFD calculations and experimental analyses *J. Fluids Eng. (Trans. ASME)* **132** 031104
[4] Borges J E 1990 A three-dimensional inverse method for turbomachinery—Part 1: theory *Trans. ASME, J. Turbomach.* **112** 346–54
[5] Borges J E 1993 A proposed through-flow inverse method for the design of mixed-flow pumps *Int. J. Numer. Methods Fluids* **17** 1097–114
[6] Brennen C E 1995 *Cavitation and Bubble Dynamics* (New York: Oxford University Press)
[7] Cao S L, Peng G Y and Yu Z Y 2005 Hydrodynamic design of rotodynamic pump impeller for multiphase pumping by combined approach of inverse design and CFD analysis *Trans. ASME, J. Fluids Eng.* **127** 330–8
[8] Crighton D G 1985 The Kutta condition in unsteady flow *Annu. Rev. Fluid Mech.* **17** 411–45
[9] Cumpsty N A 1989 *Compressor Aerodynamics* (Cambridge: Longman Scientific and Technical)
[10] Damle S, Dang T, Stringham J and Razinsky E 1999 Practical use of three-dimensional inverse method for compressor blade design *Trans. ASME, J. Turbomach.* **121** 321–5
[11] Daneshkhah K and Ghaly W 2006 An inverse blade design method for subsonic and transonic viscous flow in compressors and turbines *Inverse Problems Sci. Eng.* **14** 211–31
[12] Dang T, Damle S and Qiu X 2000 Euler-based inverse method for turbomachine blades—Part 2: three-dimensional flows *AIAA J.* **38** 2007–13
[13] Demeulenaere A and van den Braembussche R A 1998 Three-dimensional inverse method for turbomachinery blading design *Trans. ASME, J. Turbomach.* **120** 247–55
[14] Denton J D 1993 Loss mechanisms in turbomachines *Trans. ASME, J. Turbomach.* **115** 621–56
[15] Dixon S L 1998 *Fluid Mechanics, Thermodynamics of Turbomachinery* (Amsterdam: Elsevier)
[16] Drela M 1990 Viscous and inviscid inverse schemes using Newton's method *Special Course for Airfoil Design for Aeronautical and Turbomachinery Applications* AGARD Report 780
[17] van Esch B P M and Kruyt N P 2001 Hydraulic performance of a mixed-flow pump: unsteady inviscid computations and loss models *Trans. ASME, J. Fluids Eng.* **123** 256–64
[18] Hart M and Whitehead D S 1987 A design method for two-dimensional cascades of turbomachinery blades *Int. J. Numer. Methods Fluids* **7** 1363–81
[19] Hawthorne W R, Wang C, Tan C S and McCune J E 1984 Theory of blade design for large deflections—Part 1: two-dimensional cascade *Trans. ASME, J. Eng. Gas Turbines Power* **106** 346–53
[20] Ihlenburg F and Babuska I 1995 Finite-element solution of the Helmholtz-equation with high wave-number: the *h*-version of the FEM *Comput. Math. Appl.* **30** 9–37
[21] Jiang J and Dang T 1997 Design method for turbomachine blades with finite thickness by the circulation method *Trans. ASME, J. Turbomach.* **119** 539–43
[22] Kelder J D H, Dijkers R J H, van Esch B P M and Kruyt N P 2001 Experimental and theoretical study of the flow in the volute of a low specific-speed pump *Fluid Dyn. Res.* **28** 267–80

[23] Kruyt N P, Cuvelier C, Segal A and van der Zanden J 1988 A total linearization method for solving viscous free boundary flow problems by the finite element method *Int. J. Numer. Methods Fluids* **8** 351–63
[24] Labrujère T E and Slooff J W 1993 Computational methods for the aerodynamic design of aircraft-components *Annu. Rev. Fluid Mech.* **25** 183–214
[25] Omodei B J 1979 Computer solutions of a plane Newtonian jet with surface tension *Comput. Fluids* **7** 79–96
[26] Pascoa J C, Mendes A C and Gato L M C 2009 A fast iterative inverse method for turbomachinery blade design *Mech. Res. Commun.* **36** 630–7
[27] Peng G Y, Cao S L, Ishizuka M and Hayama S 2002 Design optimization of axial flow hydraulic turbine tunner—Part 1: an improved Q3D inverse method *Int. J. Numer. Methods Fluids* **39** 517–31
[28] Peng G Y, Cao S L, Ishizuka M and Hayama S 2002 Design optimization of axial flow hydraulic turbine tunner—Part 2: multi-objective constrained optimization method *Int. J. Numer. Methods Fluids* **39** 533–48
[29] Rosa Taddei S and Larocca F 2012 Potential of specification of swirl in axisymmetric CFD methods for turbine blade aerodesign *Inverse Problems Sci. Eng.* **20** 533–51
[30] Qiu X, Ji M and Dang T 2009 Three-dimensional viscous inverse method for axial blade design *Inverse Problems Sci. Eng.* **17** 1019–36
[31] Roidl B and Ghaly W 2011 Redesign of a low speed turbine stage using a new viscous inverse design method *Trans. ASME, J. Turbomach.* **133** 011009
[32] Ruschak K J 1980 A method for incorporating free boundaries with surface tension in finite element fluid-flow simulators *Int. J. Numer. Methods Eng.* **15** 639–48
[33] Saito H and Scriven L E 1982 Study of coating flow by the finite element method *J. Comput. Phys.* **42** 53–76
[34] Schlichting H and Gersten K 2000 *Boundary-Layer Theory* (Berlin: Springer)
[35] Silliman W J and Scriven L E 1979 Separating flow near a static contact-line: slip at a wall and shape of a free surface *J. Comput. Phys.* **34** 287–313
[36] Spring H 1992 Affordable quasi three-dimensional inverse design method for pump impellers *Proc. 9th Int. Pump Users Symp.* pp 97–110
[37] Spring H 1995 Judge the pump hydraulic design through numbers before you buy *Proc. 12th Int. Pump Users Symp.* pp 113–9
[38] Tan C S, Hawthorne W R, McCune J E and Wang C 1984 Theory of blade design for large deflections—Part 2: annular cascades *Trans. ASME, J. Eng. Gas Turbines Power* **106** 354–65
[39] Tuzson J 2000 *Centrifugal Pump Design* (New York: Wiley)
[40] Veress A and van den Braembussche R A 2004 Inverse design and optimization of a return channel for a multistage centrifugal compressor *Trans. ASME, J. Fluids Eng.* **126** 799–806
[41] de Vito L, van den Braembussche R A and Deconinck H 2003 A novel two-dimensional viscous inverse design method for turbomachinery blading *Trans. ASME, J. Turbomach.* **125** 310–6
[42] Wang Z M, Cai R X, Chen H J and Jia X C 2000 A three-dimensional inverse method using Navier–Stokes equations for turbomachinery blading *Inverse Problems Eng.* **8** 529–51
[43] Westra R W 2008 Inverse-design and optimization methods for centrifugal pump impellers *PhD Thesis* Department of Mechanical Engineering, University of Twente, Enschede, The Netherlands
[44] Zangeneh M 1991 A compressible three-dimensional design method for radial and mixed flow turbomachinery blades *Int. J. Numer. Methods Fluids* **13** 599–624
[45] Zangeneh M 1994 Inviscid-viscous interaction method for three-dimensional inverse design of centrifugal impellers 1994 *Trans. ASME, J. Turbomach.* **116** 280–90
[46] Zangeneh M, Goto A and Takemura T 1996 Suppression of secondary flows in a mixed-flow pump impeller by application of three-dimensional inverse design method—Part 1: design and numerical validation *Trans. ASME, J. Turbomach.* **120** 536–43
[47] Zienkiewicz O C and Zhu J Z 1992 The superconvergent patch recovery and a posteriori error estimates: the recovery technique *Int. J. Numer. Methods Eng.* **33** 1331–64